Contents lists available at ScienceDirect

International Journal of Applied Earth Observations and Geoinformation

A comparison of terrestrial and UAS sensors for measuring fuel hazard in a dry sclerophyll forest

Samuel Hillman [a,c,*], Luke Wallace [a], Arko Lucieer [b], Karin Reinke [a,c], Darren Turner [b], Simon Jones [a,c]

[a] School of Science, RMIT University, Melbourne, VIC 3001, Australia
[b] School of Geography and Environmental Studies, University of Tasmania, Hobart, TAS 7001, Australia
[c] Bushfire and Natural Hazards Cooperative Research Centre, East Melbourne, VIC 3004, Australia

A B S T R A C T

In recent years, Unoccupied Aircraft Systems (UAS) have been used to capture information on forest structure in unprecedented detail. Pioneering studies in this field have shown that high spatial resolution images and Light Detecting And Ranging (LiDAR) data captured from these platforms provide detailed information describing the dominant tree elements of canopy cover and biomass. However, to date, few studies have investigated the arrangement of vegetation elements that contribute directly to fire propagation in UAS LiDAR point clouds; that is the surface, near-surface, elevated and intermediate-canopy vegetation. This paper begins to address this gap in the literature by exploring the use of image-based and LiDAR 3D representations collected using UAS platforms, for describing forest structure properties. Airborne and terrestrial 3D datasets were captured in a dry sclerophyll forest in south-eastern Australia. Results indicate that UAS LiDAR point clouds contain information that can describe fuel properties in all strata. Similar estimates of canopy cover (TLS: 68.27% and UAS LiDAR: 64.20%) and sub-canopy cover (Elevated cover TLS: 44.94%, UAS LiDAR: 32.27%, combined surface and near-surface cover TLS: 96.10% UAS LiDAR: 93.56%) to TLS were achieved using this technology. It was also shown that the UAS SfM photogrammetric technique significantly under performed in the representation of the canopy and below canopy structure (canopy cover - 20.31%, elevated cover 10.09%). This caused errors to be propagated in the estimate of heights in the elevated fuel layer (TLS: 0.51 m, UAS LiDAR: 0.34 m, UAS SfM: 0.15 m). A method for classifying fuel hazard layers is also presented which identifies vegetation connectivity. These results indicate that information describing the below canopy vertical structure is present within the UAS LiDAR point clouds and can be exploited through this novel classification approach for fire hazard assessment. For fire prone countries, this type of information can provide important insight into forest fuels and the potential fire behaviour and impact of fire under different scenarios.

1. Introduction

Climate change is increasing fire activity across the globe, with lengthening fire seasons and corresponding increases in frequency and severity of fire events (Matt Jolly et al., 1979; Jain et al., 1979; Abatzoglou et al., 2018; Clarke et al., 2011). In the past 20 years, south-eastern Australia has seen evidence of these phenomena with wide-scale wildfire events causing significant changes in ecosystems and loss to life and property (Cameron et al., 2009; Nyman et al., 2011; Bradstock, 2009; McLeod, 2003; Ellis et al., 2004). When considering fire behaviour, it is widely understood that fuel, weather and topography dictate the movement of fire through the landscape (Sullivan et al., 2012). Of these three factors only fuel is able to be modified by land management actions (Fernandes and Botelho, 2003). Correspondingly, land management agencies are implementing fuel management programs to build ecosystem resilience and reduce risk to life and property (Duff et al., 2013, 2019; Stephens et al., 2012). An assessment of vegetation structure is therefore vital to understanding potential wildfire behaviour, potential suppression difficulty, risk to assets, and vegetation resilience, and is an important planning tool in helping to understand the complex set of factors influencing fuel management actions.

Fuel structure can be defined as the spatial arrangement of vegetation elements and be described in terms of the composition and continuity within the vertical profile (McElhinny et al., 2005; Gould et al., 2008; Hines et al., 2010; Duff et al., 2017). When assessing fuel structure a combination of direct and indirect methods have been used. Current practices around the world involve separating vegetation into several classes (Hines et al., 2010; Prichard et al., 2013; Rodríguez y Silva and Molina, 2010). Whilst these classifications differ between jurisdictions and forest types, they are often based upon distinct strata driven by height and the properties of the vegetation element as a fuel (Prichard et al., 2013). In south-eastern Australia, for instance fuel is separated into four distinct strata based on height and a separate class for bark hazard (Hines et al., 2010). Once separated, vegetation in each of these classes undergoes a fuel risk assessment based on several metrics, for example coverage of live and dead fuel, vertical continuity, height, and density (Hines et al., 2010; Gould et al., 2008).

Of particular focus in this assessment is the arrangement of fuel over the vertical profile. This type of fuel which connects vegetation from the ground to the elevated fuel layer or canopy is often referred to as ladder fuels (Menning and Stephens, 2007; Skowronski et al., 2007). These fuels have a significant influence on flame height and the rate of spread of a fire with the potential to allow a fire to travel from the surface to the crown (Hines et al., 2010; Ottmar et al., 2007; Menning and Stephens, 2007). Measuring ladder fuels is challenging and whilst a measurement of the top and bottom of the ladder fuels can be taken, these measurements do not describe the density of vegetation (Ottmar et al., 2007). From a visual assessment perspective, density is determined both by an estimate of the abundance of fuel per unit area and through an assessment of the ability of this fuel to allow fire to travel up the ladder (Ottmar et al., 2007) or a relative assessment in the terms of the difficulty for an assessor to walk through the vegetation(Hines et al., 2010). Consistent with estimating other strata of fuel, visual assessment of ladder fuels whilst quick and effective at providing a rapid overview of the fuels have been shown to be subjective and results are highly variable between assessors (Watson et al., 2012; Volkova et al., 2016; Spits et al., 2017).

Recent advancements in remote sensing allow three dimensional representations of forest structural characteristics to be accurately captured. Such representations of the forest fuel complex can in turn be used in the abstraction of fuel metrics (Hermosilla et al., 2014; Eric Rowell et al., 2016, 2020; Chen et al., 2016) and fire modelling systems (Parsons et al., 2011; Pimont et al., 2016). High resolution 3D data enable the consideration of vegetation strata classification based on a data driven approach (Wilkes et al., 2016), or considering the proximity of each point to a neighbouring set of points (Chen et al., 2016) instead of defined height thresholds (Hines et al., 2010; Gould et al., 2008) which may not be suitable for all forest types. Skowronski et al. (2007) utilised airborne lidar to detect the presence of ladder fuels in Pinelands and highlighted the potential to use binned data to detect ladder fuels. To date, there has been limited research conducted to develop quantitative measures of vegetation connectivity in Australian Eucalypt forests. Two remote sensing techniques have been utilised in the past to construct 3D representations of the environment; image-based and laser scanning.

Image-based 3D representations utilise computer vision algorithms and photogrammetric principles to construct a point cloud from highly overlapping images captured from multiple viewpoints (Dandois and Ellis, 2013; Snavely et al., 2007; Goldbergs et al., 2018). Terrestrial image-based point clouds have been successful at resolving fine fuel characteristics below 1 m in small plot areas (Hillman et al., 2019; Wallace et al., 2019; Spits et al., 2017; Cooper et al., 2017). Image-based point clouds captured from Unoccupied Aircraft Systems (UAS) have also been used to measure vegetation properties such as canopy height and cover, diameter at breast height, and stem count (Wallace and Lucieer, 2016; Puliti et al., 2019). Prior studies have shown reconstruction of below-canopy vegetation structure to be highly variable,

with some examples showing limited vegetation representation Wallace and Lucieer (2016), Graham et al. (2020).

Laser scanners measure the time of flight for a laser pulse to be reflected from a feature and return to the sensor to calculate range (Newnham et al., 2015). Light Detection and Ranging (LiDAR) from fixed wing aircraft has been used extensively for measuring forest characteristics (Hollaus et al., 2007; Höfle et al., 2008; White et al., 2013; Hill et al., 2014). Whilst this platform provides wide area observations, Terrestrial Laser Scanners (TLS), both static and handheld, are able to provide high resolution, localised LiDAR data over small areas. Previous studies have utilised TLS derived point clouds to characterise stem properties, develop allometric biomass relationships, and observe fine scale vegetation characteristics (Disney et al., 2019; Newnham et al., 2015; Calders et al., 2015). Studies investigating the capacity of LiDAR for the measurement of small structural vegetation characteristics have demonstrated the ability of point clouds to estimate fuel hazard properties (Eric Rowell et al., 2016; Hillman et al., 2019). To bridge the gap between terrestrial observations and large-scale fixed-wing airborne observations, UAS LiDAR has also been utilised to capture 3D representation of vegetation (Wallace et al., 2012, 2016; Sankey et al., 2017; Guo et al., 2017; Cao et al., 2019). Previous UAS LiDAR (low-altitude) studies have predominantly focused on replicating existing metrics from fixed-wing airborne (high altitude) point clouds (Liu et al., 2018). Studies investigating the relationship between point clouds derived from TLS and UAS point clouds have compared tree-based properties such as DBH and volume Brede et al. (2017), Brede et al. (2019), Fritz et al. (2013), Wieser et al. (2017). To the best of our knowledge there have been no comparisons of UAS point clouds with TLS point clouds for measuring fine-scale vegetation structure (less than 0.05 m).

Studies comparing active and passive sensors have noted the distinct differences in capturing technique, processing and metric generation (Wallace and Lucieer, 2016; Puliti et al., 2019; Cao et al., 2019). Most significantly, the ability for airborne LiDAR to penetrate the canopy of forest environments facilitates greater detection of below canopy vegetation elements, as well as aiding ground surface reconstruction. Whilst some UAS surveys have compared metrics from the point cloud to direct measurements from the ground (Wallace and Lucieer, 2016; Liu et al., 2018; Sankey et al., 2017), limited research has been conducted to validate below canopy structure characteristics captured from UAS platforms.

The objective of this study is to provide a comparison of image-based and LiDAR point clouds derived from terrestrial and UAS capture methods. We assess the ability of each technology to capture the ground surface, the vertical profile of vegetation, and horizontal coverage and height for different vegetation strata. This assessment is used to highlight the ability of each technology to represent the overall fuel complex. The applicability of these technologies to be used for fuel layer extraction, fuel coverage, and height mapping for local scale forest monitoring will also be discussed.

2. Materials and methods

2.1. Plot and survey design

The 'Ridgeway' study area was located south-east of Hobart in Tasmania, Australia. The predominant forest type was native dry sclerophyll eucalypt forest (Fig. 1). The dominant canopy species consisted of *Eucalyptus pulchella* trees of mixed ages and ranging in height from 4.7 m to 16.2 m. The understorey consisted of sparse low to medium height 0.5 m to 2 m shrubs, and areas of native grasses approximately 0.1 m to 0.4 m high. The study area had been subject to planned burning activities in 2016 with significant removal of vegetation below 2 m observed. 30 × 50 m plot was chosen to capture a range of overstorey and understorey conditions with data capture completed in March 2018.
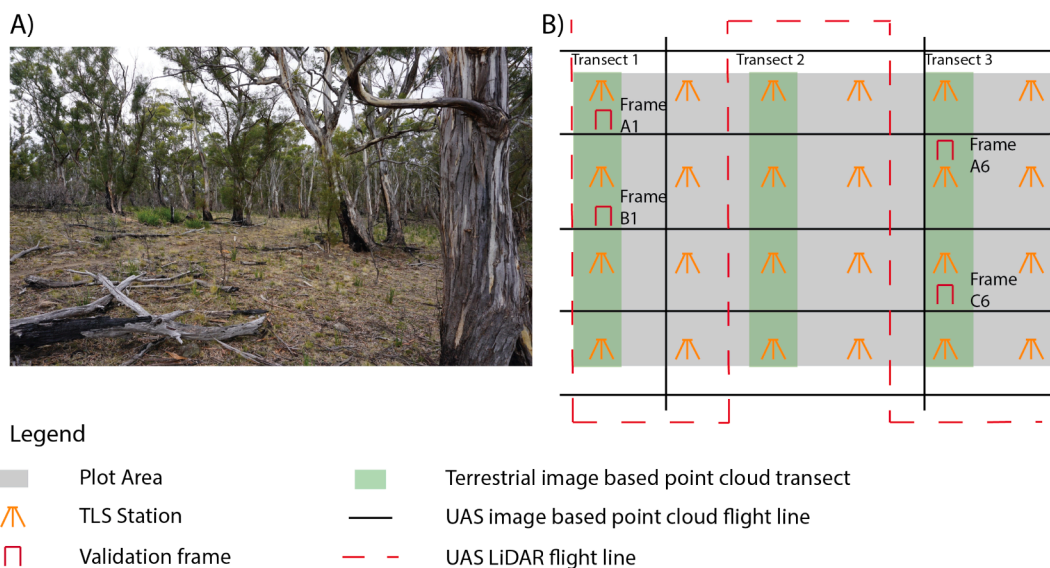
Fig. 1. (A) Photograph showing the dry eucalyptus forest in which the technology was assessed. (B) Plot layout schematic showing the relative positioning of different data capture sources.

2.2. Data collection technologies and software

2.2.1. Ground control

In order to geo-register and enable comparison of the point clouds derived from SfM work flows with the LiDAR point clouds, ground control targets were painted in a cross-hair form on the ground in locations that provided clear-sky views, and allowed a suitable point distribution for use with the SfM data. The position of these targets was observed with a Leica 1200 Global Navigation Satellite System (GNSS) receiver operating in Real-Time Kinematic (RTK) mode. This produced an absolute positional error for control of 3–5 cm. A GNSS base station remained running for the duration of the survey. The ground control targets were used as an initial basis for co-aligning all remotely sensed data.

2.2.2. UAS LiDAR data capture

LiDAR data was captured with a custom-built UAS developed at the University of Tasmania, Australia. The system consisted of a DJI M600 platform, a Velodyne Puck (VLP-16) and an Advanced Navigation Spatial Dual coupled GNSS and IMU sensor. The VLP-16 scanner features 16 scan layers with a 30° vertical Field Of View (FOV), which equates to a 15° forward and backward distribution of the scan lines in the flight direction (+15° to −15° from nadir, with scan lines separated by approximately 2°). A maximum of 2 laser returns per pulse are collected with 300,000 pulses per second for the full 360° view of the scanner. The scan angle was limited to −40° to +40° in the across-track direction (80° field-of-view) resulting in approximately 60,000 pulses per second. Flying height was 40;m above the ground level. The scanner has a horizontal beam divergence of 0.18° (3.0 mrad); vertical: 0.07° (1.2 mrad), resulting in a laser footprint of 12.6 cm by 4.9 cm on the ground. Flight lines are illustrated in (Fig. 1). The overlap between flight strips was 50%. Georeferenced LiDAR point clouds were generated using Python software code that was developed in-house specifically for UAS LiDAR processing.

2.2.3. TLS data capture

TLS data was captured using a Trimble TX8 laser scanner set to capture Level 2 quality scans (11.3 mm point resolution at a distance of 30 m). Twenty-four scans were captured in a 10 m grid pattern to allow full coverage of the plot (Fig. 1).

TLS Scans were co-registered in Trimble Realworks 10.1 using scan-to-scan matching. The quality of the matches was assessed with scans manually adjusted through the use of common features found within the point cloud. To georegister the TLS data a six parameter transformation (three translations and three rotations) was defined based on a set of common points. For this purpose, a minimum of six common features (such as tree stems) were identified in the geo-rectified UAS LiDAR and UAS SfM point clouds, and the relevant translation and rotation applied to the point cloud. Visual inspection of the point clouds was then conducted to ensure accurate co-registration. This process was repeated three times to create the most accurate co-registration of the point clouds.

2.2.4. UAS SfM data capture

Airborne imagery was captured using a DJI Phantom 4 Pro. Images were captured using the platform's integrated RGB camera. The UAS was flown at a flying height of 40 m above ground level. Flight lines were flown parallel to the 50 m side of the plot to capture 90% forward and sidelap (Fig. 1). Finally, two cross strips were flown over the 30 m side of the plots. Imagery was captured at nadir with camera settings manually set to match the prevailing light conditions at the time of capture, balancing illumination of the ground and canopy (f 3.5, shutter speed 1/1000 s, and ISO 400).

2.2.5. Terrestrial SfM data capture

Images were collected with a modified Sony Alpha 6000 camera. This camera had been converted to a full-wavelength sensor, and used a 760 nm pass-filter to limit the captured wavelengths to the edge of red and near infrared wavelengths. The near-infrared camera was chosen for terrestrial images to allow for improved discrimination between leaf litter and the bare ground. Transects were placed parallel to each other with a five metre offset between each transect across the plot (see Fig. 1). Images were captured along either side of the centreline of six 30 m transects by hand. Standing approximately 2 m from the transect centreline, images were captured with a horizontal spacing of approximately 0.2–0.3 m along the full length of the transect. Corresponding with a horizontal change in spacing, the height of the image capture cycled through heights of 1.0 m, 1.4 m and 1.8 m. This image capture sequence resulted in approximately 240 photos for each transect. Along each transect, six PVC pipes were placed approximately 5 m apart to assist image matching, and each pipe had a unique colour coded target to provide scale. Along two transects, two validation frames (see Section 2.2.7) were captured for ground validation purposes, with an additional six downward looking images over the top of the frame captured to

complete the image acquisition process.

2.2.6. Image processing UAS and terrestrial datasets

Images were downloaded from the camera(s) and processed to form a point cloud using Agisoft Metashape Professional v1.5.0 (www.agisoft.com) software (Agisoft LLc, St. Peterburg, Russia). A sparse point cloud was generated using the high quality alignment setting where common features were found within the image set. Images were then aligned based on an iterative bundle adjustment to estimate the 3D positions of the matched features. Ground control targets were then identified within the images to geo-reference the point clouds, in-turn facilitating direct comparison to point clouds derived from laser scanning. The high quality setting and mild depth filtering were then applied to generate a dense point cloud. Once point clouds were produced from the respective platforms, removal of spurious points beneath the ground was applied.

2.2.7. Validation frame

A validation frame was placed at four separate locations within the study plot area (Fig. 1) to validate the information content within terrestrial point clouds describing surface and near-surface vegetation. Each frame consisted of a 0.5 × 0.5 m quadrat on four variable height legs as described in Hillman et al. (2019). A moveable rack sitting within the frame was used to record point intercepts. The rack is designed with two vertical bars spaced 5 cm apart to ensure when inserted the rods remain closely aligned to the z-axis. A total of 64 points with the height and number of vegetation intercepts on an aluminium rod of 0.6 cm diameter were taken at known locations within the coordinate system defined by the frame. For each rod, the method outlined in (Herrick et al., 2006) for taking point intercept measurements was followed. This involves noting the height above ground, type and width of any vegetation elements intercepting the rod. The height of the rod at the bottom of the second vertical bar was also observed to determine the location of the ground within the frames coordinates system.

2.3. Ground identification and normalisation

The ability to represent a ground surface is vital when assessing the ability of each technique to characterise below canopy vegetation structure. The ground defined within the validation frame was used as the basis for validating the ground points within the near-infrared (NIR) terrestrial image-based point clouds. The NIR point clouds were first filtered for ground points using the in-built ground filter within Agisoft Metashape (Agisoft LLC, St. Petersburg, Russia). The filter within Metashape was applied to the point cloud with a resolution of 0.5 m, distance threshold of 0.05 m and angle threshold of 15° (Agisoft LLC, St. Petersburg, Russia). Following the application of the Agisoft Metashape filter, ground points were further refined based on their intensity within the point cloud. Using visual inspection of the point clouds by three assessors, a threshold was applied to the NIR value attributed to each point in order to eliminate those points that originated from vegetation but were identified as ground in the original filter. This threshold value was optimised based on the reduction of the Root Mean Square Error (RMSE) between the validation frame measurements of the ground and near-infrared point cloud. For areas outside of the validation frame, the threshold value was validated using visual assessment by three assessors.

Noise detection and removal was completed on all point clouds to remove spurious points beneath the ground. Ground points were identified in the TLS, UAS LiDAR and UAS image-based point clouds using the Cloth Simulation Filter (CSF) outlined in Yilmaz et al. (2018). For each technology, the ground points were identified using the CSF filter and were processed to form a Triangular Irregular Network (TIN). The height of the TIN facet at the centre of each cell was then attributed to a 0.02 m Digital Terrain Model (DTM). Three terrestrial NIR image-based transect areas were extracted from the TLS, UAS LiDAR and UAS image-based point clouds respectively. The settings for the CSF filter were

optimised for each technology separately, minimising RMSE between the DTM of the reference near-infrared transect and the DTM of each respective technology. These optimised parameters are provided in Table 1. The point cloud was normalised based on each point's height above the DTM, thereby providing a representation of the point cloud in relation to the ground.

2.4. Fuel strata classification

2.4.1. Voxelisation

A voxel is the 3D equivalent of a pixel, where space is described in x,y and z and the size of the grid cells determining the resolution of the 3D grid (Vosselman et al., 2004). The point cloud density was normalised in a 2 cm voxel space before further analysis was completed. Variations in the point density across the plot due to topography, flight path selection and sensor angle were accounted for through this process. This allowed the handheld SfM, TLS, UAS LiDAR and UAS SfM point clouds to be compared, where each point cloud was transformed into a binary voxel model indicating vegetation presence or absence.

2.4.2. Vegetation classification

Information about the vertical and horizontal variation in fuel structure and associated hazard allows for a greater understanding of potential risk. A novel approach considering connections between voxel layers was applied in order to extract information describing the overall fuel complex. This approach considers any fuel that is vertically connected to a higher layer to be part of that higher layer.

The first step is to apply a dilution to the voxel space using a spherical structure element. The size of this element was optimised based on visual inspection for each technology. This creates a voxel space in which the originally occupied voxels become vertically connected to the voxels directly above them and the voxels on either side. Following, horizontally connected voxels in the top most layer are assigned a unique identifier. These identifiers are then passed to any horizontally coincident voxel segments in the next layer down. Any new segments are labeled with their own unique identifier. Where two segments from an upper layer partially overlap the same contiguous segment in the subsequent layer, a flood fill approach using the upper layer segments as seeds is applied. This process is continued until the bottom voxel layer is reached.

Once all voxels had been assigned to an object, the object is assigned the height of the first (or highest) voxel layer in which it was identified. This allows objects to be allocated to a fuel strata. For this study, although there are no fixed height thresholds defined in the literature for describing fuel strata, we applied an approach consistent with fuel studies in eucalypt forests. This created four classes which capture the surface and near-surface combined fuel layer (<0.6 m), elevated (0.6–3 m), intermediate (3–5 m) and canopy (>5 m) fuel layers(Hines et al., 2010; Gould et al., 2008) (Fig. 2).

Finally, points originating from stems were separated from the canopy class. This separation was completed by identifying the canopy base height (CBH) across the plot. The method presented in Wallace et al. (2014), which aims to determine CBH based on the area filled by points within each vertical voxel layer, was adapted for this purpose. In brief, this method uses the 2D alpha shape, constructed with an alpha value of

Table 1
Filter settings applied to the Cloth Simulation Filter for SfM and TLS point clouds to identify ground points in the study plot.

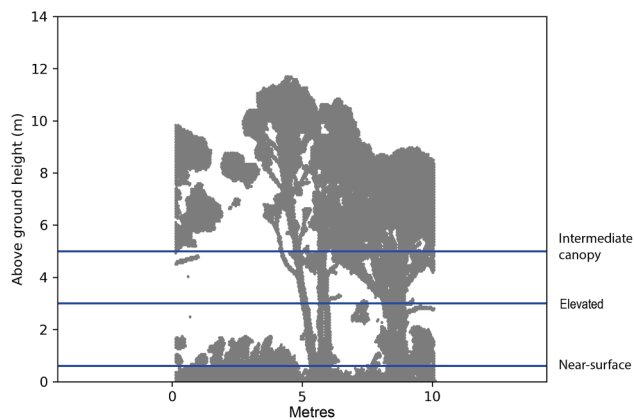|	TLS	UAS LiDAR	UAS SfM
Cloth Resolution (m)	0.09	0.09	0.09
Class Threshold (m)	0.03	0.05	0.03
Rigidity	3	1	2
Time Step	0.4	0.4	0.4
Iterations	1000	1000	1000

Fig. 2. Height thresholds used to extract different fuel strata (based on Hines et al., 2010; Gould et al., 2008) and applied to a portion of the study area.

0.2 for UAS LiDAR and UAS SfM and 0.05 for TLS point clouds, for each set of points within a voxel layer. The area of each alpha shape is then calculated. CBH is finally determined as the lowest voxel layer where the next 10 higher layers have an alpha shape area greater than the 25*th* percentile area calculated from all layers. In contrast, to Wallace et al. (2014) who used points from individually segmented trees to calculate CBH, this approach was applied based on the identification of stems from the canopy class in clusters of points with above ground height (AGH) occurring between 2.0 m and 2.2 m above the ground. Clusters were identified by finding distinct alpha shapes formed from these points. Next, all canopy points were associated to the nearest cluster. The CBH was then determined for each set of points with all points with an AGH below CBH reclassed as stem/bark fuel.

2.4.3. Analysis of fuel strata information

In order to assess the ability of each point cloud technology to represent below canopy vegetation structure, a four-stage hierarchical validation and inter-comparison strategy was used. Firstly, the point intercept frame was used to assess the quality of the representation of the ground and vegetation in the TLS and NIR terrestrial image-based point clouds. The error in ground height was summarized using measures of difference such as Root Mean Square Error (RMSE). Assessing the quality of the raw point cloud data in representing the vegetation within the validation frame, the presence or absence of voxel data was directly compared. As there is likely to be a higher number of empty voxels in most of the collected datasets, a Matthew Correlation Coefficient (MCC) was utilised following the approach of Gawel et al. (2016), Aijazi et al. (2013).

Secondly, three transects of 20 m in length and approximately 2.5 m in width were extracted from the normalised TLS, UAS LiDAR and UAS image-based point clouds of the plot to align with the three NIR terrestrial image-based point clouds. The length of transect was reduced due to the ends of the terrestrial image-based point clouds not fully extending to the plot boundaries at the time of field capture. From here the ability of each technology to represent the ground surface was assessed across each of the three transects, with the differences between DTM grids (resolution of 0.1 m) of the respective technology and the NIR image-based point cloud summarized using RMSE and Mean Absolute Error (MAE).

Thirdly, these transects were then used to compare surface and near-surface (vegetation below 0.6 m) cover and height metrics from the TLS, UAS LiDAR and UAS SfM to the NIR terrestrial image-based point cloud transects (resolution of 0.1 m).

Finally, metrics were calculated at the plot level, including percentage cover and height estimates which were derived from the classified point clouds at the whole plot scale based on a 0.1 m grid size. In order to investigate the impact of canopy on the ability of each

technology to represent below canopy vegetation, the plot was tiled into 10 m tiles with canopy cover calculated on each tile. The tiles with the second highest, second lowest and median canopy cover were analysed by calculating the Above Ground Height (AGH) percentiles (25th, 50th, 95th) for heights above 0.6 m.

3. Results

3.1. TLS and terrestrial image-based point cloud validation

TLS and Terrestrial NIR image based point clouds were validated using the manual grid-intercept measurements for their ability to represent the ground and vegetation elements below 1 m. Point clouds derived from both the TLS and the NIR terrestrial imagery demonstrate correspondence to validation measurements, with RMSE of 0.008–0.021 m reported for the ground variable and vegetation height (Table 2). The MCC results also demonstrate that both the TLS and the terrestrial image-based point clouds were able to characterise the fine fuel structure beneath 1 m. Lower MCC can be attributed to grass with blade widths smaller than 5 mm not being resolved in the image-based point clouds, particularly in frame A1 and frame B1.

3.2. Inter-comparison of ground descriptions

Point clouds derived from terrestrial NIR imagery were compared to point clouds derived from TLS, UAS LiDAR and UAS SfM to assess the accuracy of ground detection. Minimal differences were observed between the ability of each technology to estimate ground surfaces across the three transects in comparison to the reference NIR terrestrial SfM point clouds. The smallest errors in ground surface reconstruction were seen in transect 1 with RMSE between 0.02 m and 0.06 m (Table 3). The greatest level of discrepancy was observed in transect 3 with RMSE between 0.03 m and 0.10 m (Table 3). UAS-LiDAR shows a wider spread of error and an overall trend to underestimate the ground compared to TLS and UAS image based point clouds (Fig. 3). This underestimation of the ground is in contrast to a positive error distribution of TLS point clouds. (Fig. 3). It should be noted, that filtering of spurious points beneath the ground was conducted on UAS image based point clouds which if left in would negatively impact the ground reconstruction and increase error.

3.3. Inter-comparison of surface and near-surface vegetation representation

Transects were extracted from the TLS, UAS LiDAR and UAS SfM point clouds which were compared to terrestrial NIR SfM point clouds for their ability to represent surface and near-surface vegetation (defined height threshold of 0.6 m). Visual assessment of the point clouds demonstrate that terrestrial NIR SfM point clouds provide a representation of the fuels as captured in the TLS point clouds (Fig. 5). Despite the lower point density, the UAS LiDAR point cloud provides an accurate representation of vegetation close to the ground. Very few points were identified in the UAS SfM reconstruction originating from vegetation close to the ground.

With the ground points removed, percentage cover of combined surface and near-surface vegetation was similar across all transects and technologies. The exception is UAS SfM which is significantly different and shows a large variation between the transects (Table 4). This relationship is present in transects with minimal vertical complexity - for example transect 1, and the more vertical complex transect 3 (Fig. 4). UAS image-based point clouds provided a lower estimate of vegetation cover in comparison to other technologies in all transects.

Image-based point clouds had lower mean heights with higher standard deviations relative to the means. This is in contrast to point clouds derived from active sensors which had higher mean heights with lower standard deviations relative to the respective mean heights

Table 2

Summary of reference frame measurements in comparison to terrestrial image-based point clouds.

Frame	RMSE (m)		mean height (m)			std.dev height (m)			MCC	
	SfM	TLS	Ref.	SfM	TLS	Ref.	SfM	TLS	SfM	TLS
Frame A1	0.009	0.008	0.009	0.003	0.001	0.020	0.037	0.007	0.48	0.46
Frame B1	0.017	0.021	0.030	0.013	0.008	0.043	0.069	0.023	0.41	0.40
Frame A6	0.008	0.012	0.089	0.096	0.180	0.181	0.196	0.238	0.56	0.49
Frame C6	0.019	0.021	0.024	0.016	0.014	0.035	0.026	0.038	0.51	0.48

Table 3

Summary of error distribution for ground generated from the respective TLS, UAS LiDAR, UAS image-based point clouds and terrestrial image-based point clouds for all transects.

		TLS	UAS LiDAR	UAS SfM
Transect 1	RMSE (m)	0.02	0.06	0.02
	MAE (m)	0.02	0.05	0.01
Transect 2	RMSE (m)	0.03	0.07	0.03
	MAE (m)	0.02	0.06	0.02
Transect 3	RMSE (m)	0.03	0.10	0.03
	MAE (m)	0.02	0.08	0.02

Fig. 4. Comparison of surface and near-surface fuel height in transect 2 between TSfM, TLS, UAS LiDAR and UAS SfM dervied point clouds.
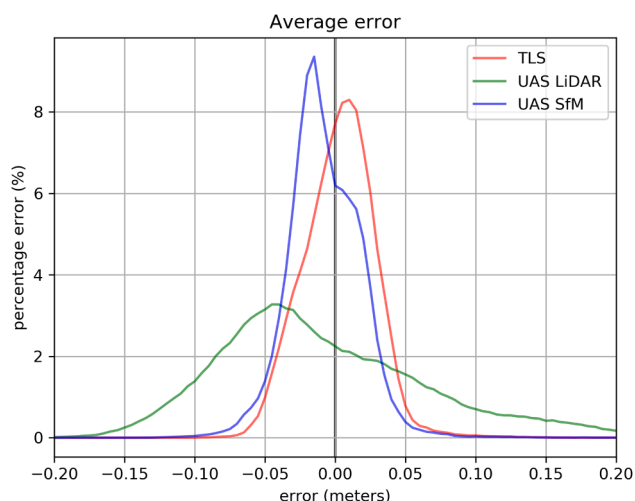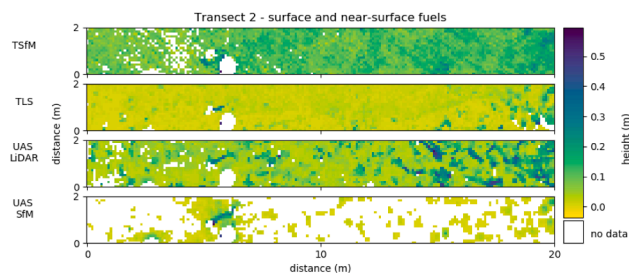

Fig. 3. Histograms showing the error between the terrestrial image based point cloud defined ground surface and the three other technologies.

Table 4

Summary of percentage vegetation cover, mean height (m) and standard deviation (m) of the combined surface and near-surface vegetation layers (with ground points removed) in the three transects across the study plot.

		Terrestrial SfM	TLS	UAS LiDAR	UAS SfM
Transect 1	Cover (%)	94.90	97.85	95.23	20.70
	Mean Height (m)	0.01	0.06	0.11	0.01
	Std Deviation (m)	0.02	0.05	0.04	0.02
Transect 2	Cover (%)	96.10	93.56	92.00	25.14
	Mean Height (m)	0.02	0.08	0.11	0.02
	Std Deviation (m)	0.03	0.08	0.04	0.05
Transect 3	Cover (%)	93.00	93.63	94.38	45.28
	Mean Height (m)	0.03	0.07	0.15	0.03
	Std Deviation (m)	0.04	0.07	0.05	0.05

(Table 4). When combined with the evidence that UAS LiDAR point clouds have a lower estimate of the ground surface, this suggests that UAS LiDAR point clouds are not detecting vegetation features close to the ground.

3.4. Fuel strata classification

After applying the classification algorithm to each of the respective point clouds, the different strata were analysed (Fig. 6). TLS and UAS LiDAR point clouds provided similar canopy cover estimates 68.27% and 64.20% respectively (Fig. 7). UAS image-based point clouds provided a limited description of canopy giving the lowest cover estimate of 20.31% (Table 5). Despite the discrepancy in cover, the mean height for canopy fuel of UAS image-based point clouds (9.81 m) was similar to the mean height derived from the TLS (9.69 m) and UAS LiDAR (9.75 m). A similar pattern where active sensors had higher cover estimates in comparison to passive sensors in classifying the canopy was seen when describing stem coverage across the plot (UAS LiDAR: 11.15%, TLS: 11.02%) in comparison to UAS SfM (3.95%). The mean height of the stems layer was measured to be higher in the UAS LiDAR than the TLS point clouds and UAS SfM (UAS LiDAR: 3.21 m, TLS: 2.82 m, UAS SfM: 1.91 m).

Cover estimates for the intermediate canopy were found to be different between sensors. TLS point clouds had the highest reported cover of 10.41%. Airborne sensors had lower reported intermediate canopy cover compared to TLS with the UAS LiDAR capturing 5.90% and UAS SfM capturing 2.18% coverage. Mean heights reported for the intermediate canopy layer from the UAS LiDAR and TLS point clouds were also higher (UAS LiDAR: 2.92 m, TLS: 3.43 m) than UAS SfM (1.15 m).

Similar to the intermediate canopy layer, cover estimates for the elevated layer varied between sensors and sampling technique. The TLS point clouds reported the highest cover 44.94%. UAS LiDAR point clouds captured 32.27% and UAS SfM resolved significantly less vegetation in this strata with 10.09%. Mean height estimates were highest in the TLS point clouds 0.51 m, followed by UAS LiDAR 0.34 m suggesting that the elevated vegetation is connected through to the ground. The passive sensors recorded a lower mean height of 0.15 m.

3.5. Vertical structure

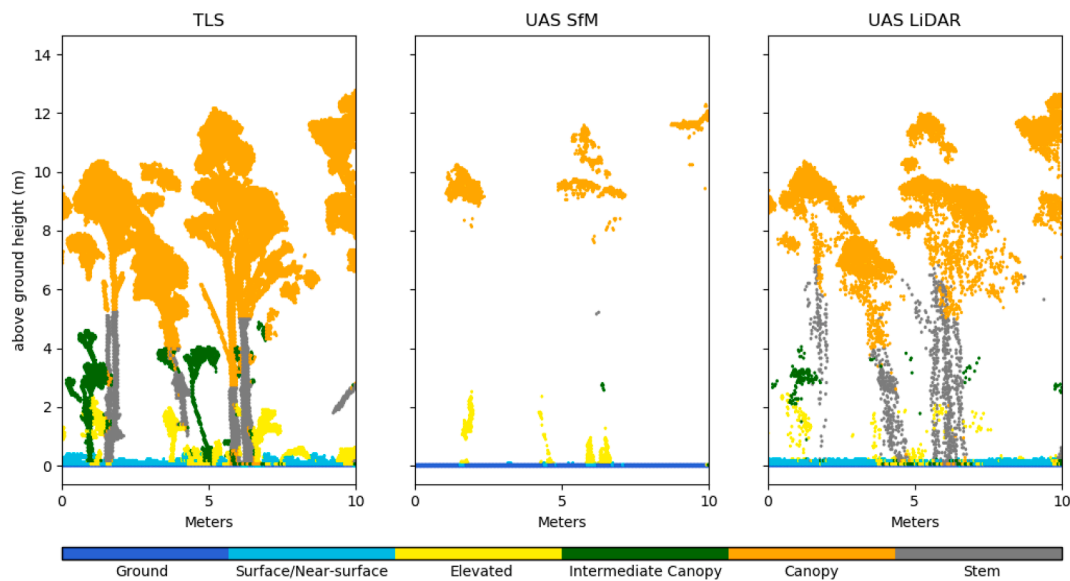Visual inspection of the point clouds suggest that TLS and UAS LiDAR

Fig. 6. Side view transect through a section of the study plot demonstrating the raster pouring classification of vegetation into canopy, stems intermediate canopy, elevated, surface/near-surface and ground layers.
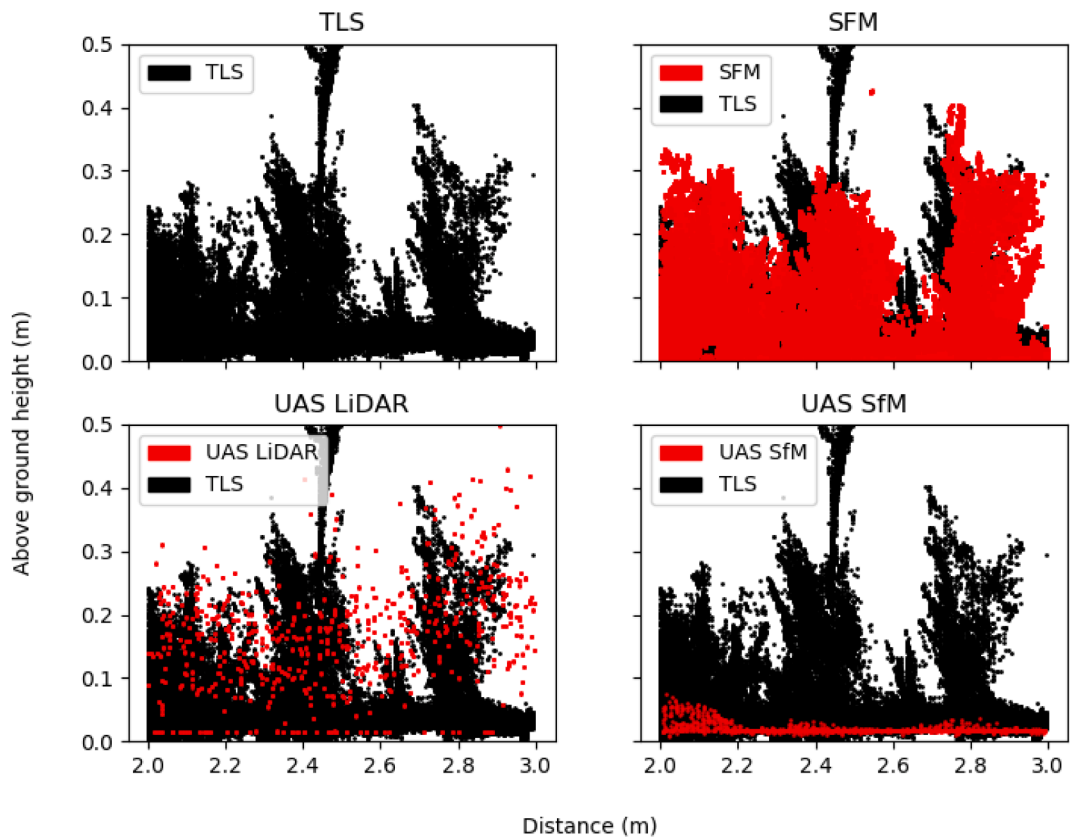

Fig. 5. Comparison of point clouds showing surface and near-surface fuel composition in a section of transect 2.

derived point clouds describe the full profile of the vegetation structure across the study area. This is highlighted in Fig. 8, which shows examples of the efficacy of each technology in areas of low (27%), moderate (55%) and high canopy cover (66%). TLS and UAS LiDAR appear to represent the canopy elements most accurately, with UAS image-based point clouds providing only partially reconstructed canopy elements (Fig. 7). This is also reflected in the 90th percentile heights in the high and low cover tiles. In the medium cover tile, UAS SfM had a higher 90th

percentile height than the TLS and UAS LiDAR point clouds.

The vegetation beneath the canopy is resolved successfully in the TLS point clouds. Spurious points are present in the TLS point clouds which could be from partial reflection or trailing points from other vegetation elements (Fig. 8). Similarly, the UAS LiDAR point clouds appear to capture the full vegetation profile. UAS LiDAR derived point clouds have higher 25th and 50th percentile heights than TLS derived point clouds (Table 6). Despite similar estimates of percentiles, visual inspection of
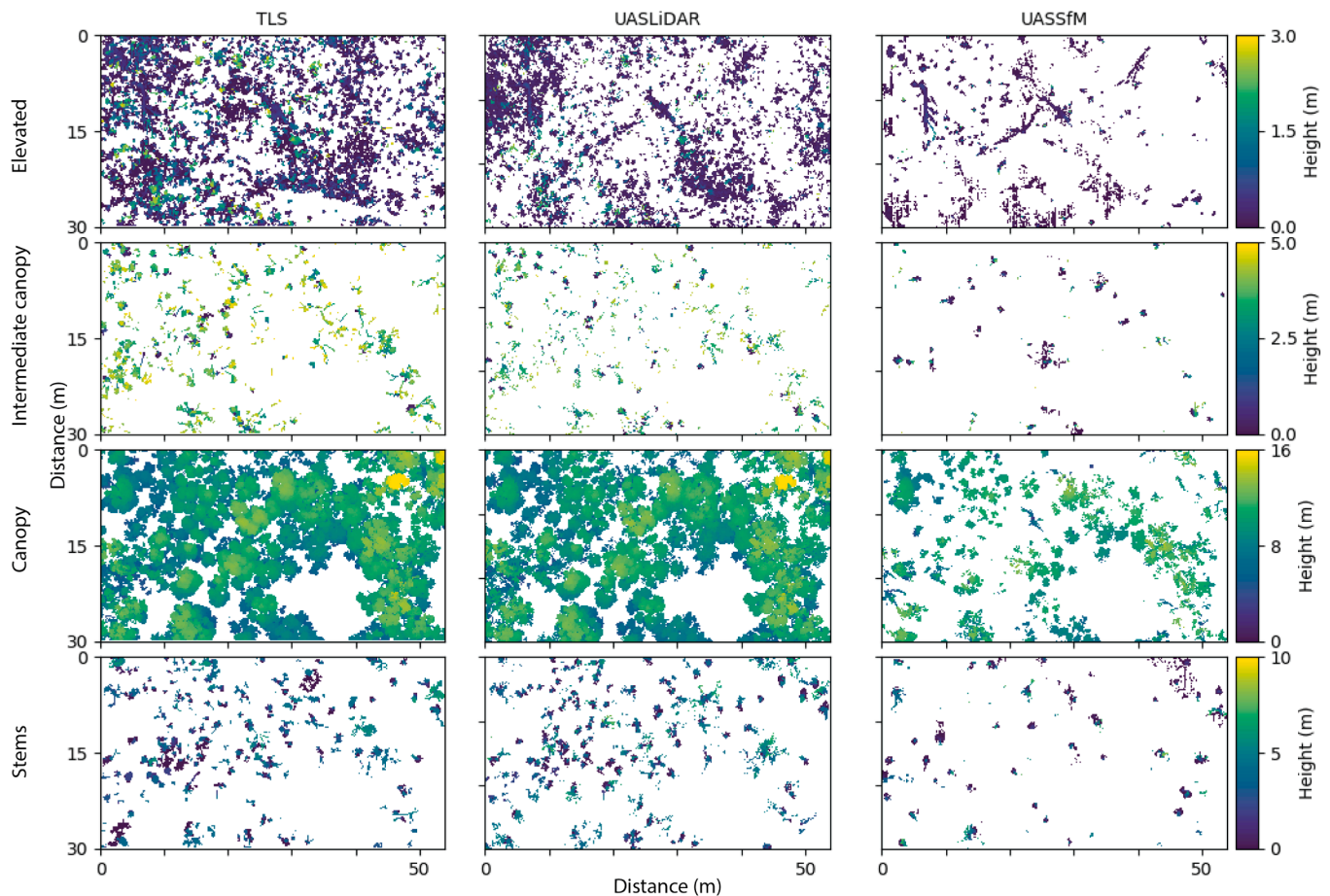
Fig. 7. Maps of the study plot showing the distribution of height for the canopy, intermediate canopy, elevated and stems layers as derived for each of the TLS, UAS LiDAR and UAS image-based point clouds.

Table 5
Summary of percentage vegetation cover, mean height (m) and standard deviation (m) for each of the canopy, intermediate canopy and elevated vegetation classes (with ground points removed) for the study plot.

Class		TLS	UAS LiDAR	UAS SfM
Canopy	Cover (%)	68.27	64.20	20.31
	Mean height (m)	9.69	9.75	9.81
	Std Deviation (m)	2.07	2.01	1.77
Intermediate Canopy	Cover (%)	10.41	5.90	2.18
	Mean height (m)	3.43	2.92	1.15
	Std Deviation (m)	1.19	1.37	1.47
Elevated	Cover (%)	44.94	32.27	10.09
	Mean height (m)	0.51	0.34	0.15
	Std Deviation (m)	0.62	0.47	0.32
Stems	Cover (%)	11.02	11.15	3.95
	Mean height (m)	2.82	3.21	1.91
	Std Deviation (m)	1.96	2.10	2.32

the UAS image-based point clouds resolved limited fine fuel structure beneath the canopy.

4. Discussion

The results presented highlight the ability of respective image-based and LiDAR technologies to resolve point clouds in a dry sclerophyll forest environment when captured from the ground or from the air. Although both the active and passive sensors were able to construct a point cloud, the information content able to be extracted, especially

beneath the canopy, varied considerably. This work supports the findings of Wallace and Lucieer (2016),Puliti et al. (2019) and Cao et al. (2019) who compared both active and passive sensors on UAS to capture point clouds for the measurement of forest characteristics (height, density and canopy information). This work extended these comparisons by comparing the different height and cover metrics from terrestrial and UAS mounted sensors in a dry eucalypt forest in the context of fuel management.

The detection of ground plays a significant role in determining the accuracy of height models. Similar to prior work (Hillman et al., 2019) utilising RGB images, ground surfaces derived from NIR terrestrial image-based point clouds had a strong relationship to directly measured ground points. The ground surface generation process utilising NIR point clouds presented in this paper provides a simple workflow to represent this layer. Whilst still requiring tuning of the threshold value through visual inspection, the results from this study demonstrate that this approach represents an accurate method to classify points originating from the ground.

When creating the DTMs, each technology was influenced by noise within the point cloud, classification of ground points and sensor type. The point clouds derived from the UAS LIDAR in this study exhibited greater error in the ground definition which can be attributed to noise in the point cloud. This is consistent with Salach et al. (2018) who, when using a similar UAS LiDAR system, showed error in ground surface measurements increasing as vegetation cover increased. Contrary to Salach et al. (2018), who used GNSS-RTK as reference for assessing DTM accuracy, our results show that the ground definition from UAS image-based point clouds was more accurate than those derived from UAS LiDAR. The accuracy of the ground provided by UAS-SfM is dependent
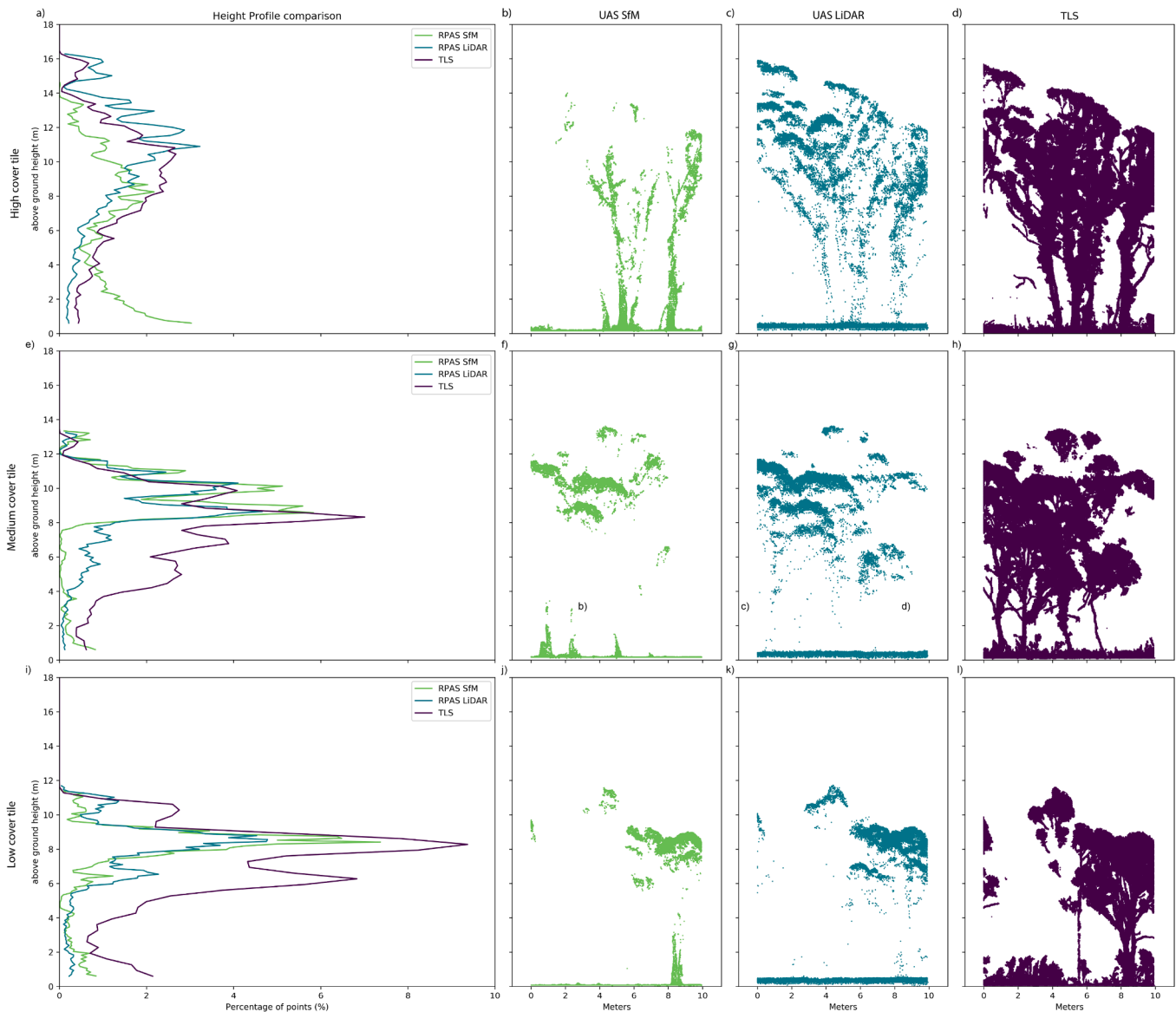
Fig. 8. Vertical structure comparison for heights above 0.6 m between point clouds derived from TLS, UAS LiDAR and UAS SfM. Three sites were delineated by a high canopy cover (66 percent) site (a, b, c, d), moderate canopy cover (55 percent) site (e, f, g, h) and low canopy cover (27 percent) site (i, j, k, l).

Table 6

Percentile height comparison for heights above 0.6 m between point clouds derived from TLS, UAS LiDAR and UAS SfM. Three sites were delineated by a high canopy cover (66 percent) site, moderate canopy cover (55 percent) site and low canopy cover (27 percent) site.

Cover Class		TLS	UAS LiDAR	UAS SfM
High	90th Percentile	12.61	13.92	10.99
	50th Percentile	9.09	10.72	6.95
	25th Percentile	6.87	8.52	2.67
Medium	90th Percentile	10.24	10.97	11.11
	50th Percentile	7.88	8.99	9.41
	25th Percentile	5.75	7.97	8.68
Low	90th Percentile	9.80	10.33	9.31
	50th Percentile	7.56	8.31	8.37
	25th Percentile	5.98	6.81	7.47

on canopy cover and density of vegetation beneath the canopy as shown in Wallace et al. (2019). It is relevant in the context of this comparison that filtering of spurious points beneath the ground had to be applied to

the UAS image-based point clouds.

The ability of the respective technologies to resolve fine-scale vegetation in the surface and near-surface strata (0–0.5 m) varied considerably. This strata were the only strata in which validation data was available. TLS and terrestrial SfM point clouds were both able to represent fine scale vegetation at the frame scale. This is consistent with other studies that have resolved fine-scale shrubs successfully from these technologies (Loudermilk et al., 2009; Cooper et al., 2017; Hillman et al., 2019). This relationship was not as strong over the entire transect where the terrestrial SfM point clouds had a lower mean height in comparison to the TLS point clouds. The dense scanning pattern and sensor resolution of the TLS (0.011 m point spacing at 30 m for single scans) allowed for complete reconstruction of the vegetation at this strata. Despite a greater point spacing compared to TLS point clouds, similar estimates of cover in the surface and near-surface layers were achieved with UAS LiDAR. Overestimation of height from UAS LiDAR in this strata is likely to be an artefact of the type of sensor used. The size of the footprint in relation to the size of the features and the geometric error could lead to under representation of small features near the ground. In this study, UAS image-based point clouds significantly

underestimated the cover of surface and near-surface vegetation along each transect. It is expected that occlusion from the forest canopy causing poor image geometry and reconstruction of the surface and near-surface vegetation could contribute to this underestimate. In addition, smoothing effects of algorithms within point cloud reconstruction could also negatively impact the ability of the processing software to represent this strata of vegetation. Environmental factors such as the movement of vegetation with small mass and fine geometrical scale will mean that vegetation elements are unable to be tracked between images and therefore not represented in the final point cloud (Cooper et al., 2017; Hillman et al., 2019).

Canopy reconstruction using UAS image-based point clouds is variable with some parts of the canopy unable to be reconstructed accurately using standard image-based photo matching and point cloud generation algorithms. Environmental conditions such as wind and sun exposure in combination with technical factors of camera overlap, spectral properties and pointing angle all contribute to the ability to reconstruct the canopy of the vegetation using image-based point clouds and potentially highlight the need for a higher resolution camera for capturing images in this environment (Puliti et al., 2019; Goodbody et al., 2019; Fletcher and Mather, 2020). Although not utilised in this study, the preservation of spectral information in UAS image-based point clouds may provide an additional source of information in detecting change especially from fire activity.

The representation of vegetation across the vertical profile varied considerably between the active and passive sensors. Whilst percentile heights were similar between TLS, UAS LiDAR and UAS SfM, visual inspection of the point clouds showed UAS SfM to perform poorly in resolving the vertical structure. Despite vegetation in these layers being present in the images, it was not entirely resolved in the point cloud. Similar to the representation of near to ground vegetation and consistent with other studies in forests, wind and the fine-scale nature of vegetation do not allow for reconstruction of these vegetation elements (Cooper et al., 2017; Hillman et al., 2019). Another contributing factor to the poor reconstruction of the vegetation in the dataset used in this study may be the sensor type. Imagery captured with a larger sensor could potentially assist with the reconstruction of below canopy vegetation. Larger sensors have greater pixel spacing and record a larger dynamic range allowing for improved distinction between vegetation elements and in turn aid their reconstruction (Santosi et al., 2017).

In contrast, the use of LiDAR from the ground or air facilitated a more complete reconstruction of the vegetation elements in the vertical profile. Point clouds derived from Terrestrial Laser Scanners have been previously shown to produce a high correlation between manual structure measurements and point cloud reconstructions and characterise individual plant structure more accurately (Olsoy et al., 2014; García et al., 2011). As noted in Wallace and Lucieer (2016) and Puliti et al. (2019) the penetration of the active sensor provides better resolution of fine-scale vegetation structure. Despite a lower point density in the UAS LiDAR (approx. 330 points/m^2) a comparison to TLS (approx. 950,000 points/m^2 points derived point clouds show that UAS LiDAR point clouds contain information that can describe fuel properties both in terms of coverage across the study area and in the vertical profile (Tables 3 and 6).

In this study, a raster pouring method was used to characterise elements of connected vegetation. Thresholds were applied from fuel management literature (Gould et al., 2008; Hines et al., 2010). These boundaries of transition influence the beginning of new layers, with connected vegetation elements being attributed their classification based on the height of the maximum voxel layer in which they occur. In the chosen study site, these thresholds were deemed appropriate for the relatively even aged stand with clear separation between the elevated fuel layer and the canopy. However, in areas where there is more complex vegetation arrangement, a data driven approach to defining layers as shown in Wilkes et al. (2016) may be more effective at defining the vegetation layers. An important consideration when applying a raster pouring approach to identify connectivity is the potential to under-represent a given stratum element. When raster pouring was applied to airborne derived point clouds, there was less intermediate canopy identified (UAS LiDAR: 5.90%) in comparison to TLS point clouds which classified 10.41% of the plot as intermediate canopy. Under representation may be caused by the settings (e.g. dilution element size) for the raster pouring causing vegetation in this strata to be mis-classified. Additionally, the technology used to derive the point cloud may not capture this vegetation information; this is evident in the UAS SfM derived point clouds.

The advantages of applying a raster-pouring approach to classifying vegetation can be viewed in the context of fire development where vertically connected vegetation elements (ladder fuels) contribute to significant increases in fire activity (Kilgore and Sando, 1975; Cruz et al., 2010; Sullivan et al., 2012; Cruz et al., 2017). Approaches to quantify ladder fuels in the past have typically combined qualitative and quantitative approaches to measuring fuels (Ottmar et al., 2007; Menning and Stephens, 2007; Prichard et al., 2013) with some preliminary studies utilising remote sensing to measure canopy base height, percentage cover below canopy or fuel gaps (Kramer et al., 2014; Maguya et al., 2015; Kramer et al., 2016; Jarron et al., 2020; Skowronski et al., 2007). Similar to the work presented by Skowronski et al. (2007), the approach outlined in this study allows for the identification and quantitative representation of ladder fuels independent of forest type. A key aspect of this work is the separation of the stem from the canopy elements. This approach makes the raster-pouring method suitable to a diverse array of landscapes where the fuel on the stem does not contribute to fire behaviour. In landscapes where there is fine bark fuel attached to the stem, further investigation into separating large woody structure from this fuel is required.

More broadly, the application of this research in fire management can be seen directly and indirectly. A direct application is in the use of point clouds to provide accurate measurements of cover and height for different strata across the plot and to subsequently calculate fuel hazard at a particular site. The use of point clouds provides a repeatable and robust method of fuel hazard assessment in comparison to current visual techniques. Indirectly, fuel hazard assessments derived from point clouds can be used to improve the accuracy of fuel modelling and in-turn fire simulations. Prior research utilising point-based visual fuel hazard assessments and landscape environmental drivers to predict fuel hazard across a region have shown promising results (Jenkins et al., 2020; McColl-Gausden et al., 2020). However, variability from visual fuel hazard assessments are likely to contribute to inaccurate fuel predictions within these models (Spits et al., 2017; Watson et al., 2012; McColl-Gausden et al., 2020; Jenkins et al., 2020). With the repeatable estimates of hazard from UAS LiDAR or TLS point cloud, it is predicted that a more accurate fuel hazard prediction may be reached.

The operational viability of each technique for land managers is an important element to consider. The total capture time for TLS data was approximately 2 h, with a processing time for all scans of approximately 4 h. The UAS LiDAR data capture took approximately 13 min, and approximately 4 h to process once GPS base station data were acquired. The UAS image-based point cloud were captured in approximately 20 min, and took approximately 8 h of processing. The time of processing is also balanced against the need for expertise in processing the data and each of these techniques requires specialist input.

Finally, an ensemble or combination of these techniques may be seen as appropriate for land managers wanting to analyse below canopy structure. It may be necessary to use TLS to obtain high density detailed information, capturing the complete profile of the vegetation initially, with broader areas able to be captured using UAS. Using the rapid collection of UAS platforms allows for the testing of different landscape management practices, and also enables provision for potential longitudinal studies of the examined areas.

5. Conclusion

The rapid development of both active and passive remote sensing technologies for forest structure characterisation means that there is now capacity to generate more accurate representations of below-canopy structure that are commensurate with recent developments and data input requirements in fire behaviour modelling. This research demonstrates that image-based and LiDAR point clouds provide a method for capturing canopy and vertical structure information in the context of a dry sclerophyll eucalypt forest. In particular, UAS LiDAR provided accurate estimates of canopy cover in comparison to TLS (TLS: 68.27% and UAS LiDAR: 64.20%) and sub-canopy cover (Elevated cover TLS: 44.94%, UAS LiDAR: 32.27%, combined surface and near-surface cover TLS: 96.10%, UAS LiDAR: 93.56%). Consideration must be given to the purpose of the assessment along with landscape characteristics when deciding on sensor selection. The scale of assessment and metrics to be extracted from point clouds are vital decision points when choosing a platform to yield accurate, repeatable, timely and efficient measurement of vegetation structure. The method presented in this research to identify vegetation connectivity demonstrates the potential of 3D remote sensing in identifying new fuel hazard metrics. The direct application of this research into fire management can be realised in the form of deriving estimates of hazard from these measurements providing forest policy makers and managers with the information required to make informed decisions about existing and future management strategies.

Data Access

Data products used in the generation of this review paper are able to be accessed via (https://doi.org/10.6084/m9.figshare.c.5015252).

CRediT authorship contribution statement

Samuel Hillman: Conceptualization, Data curation, Formal analysis, Investigation, Methodology, Validation, Visualization, Writing - original draft. **Luke Wallace:** Conceptualization, Data curation, Formal analysis, Investigation, Methodology, Supervision, Writing - review & editing. **Arko Lucieer:** Conceptualization, Data curation, Writing - review & editing. **Karin Reinke:** Conceptualization, Methodology, Project administration, Supervision, Writing - review & editing. **Darren Turner:** Conceptualization, Data curation, Writing - review & editing. **Simon Jones:** Conceptualization, Methodology, Project administration, Supervision, Writing - review & editing.

Declaration of Competing Interest

The authors declare that they have no known competing financial interests or personal relationships that could have appeared to influence the work reported in this paper.

Acknowledgements

Appendix A. Supplementary material

Supplementary data associated with this article can be found, in the online version, at https://doi.org/10.1016/j.jag.2020.102261.

References

Abatzoglou, John T., Park Williams, A., Boschetti, Luigi, Zubkova, Maria, Kolden, Crystal A., 2018. Global patterns of interannual climate–fire relationships. Glob. Change Biol. 24 (11), 5164–5175.

Aijazi, A.K., Checchin, P., Trassoudaine, L., 2013. Detecting and updating changes in lidar point clouds for automatic 3D urban cartography. ISPRS Ann. Photogramm. Remote Sens. Spatial Inform. Sci. 2 (5W2), 7–12. https://doi.org/10.5194/isprsannals-II-5-W2-7-2013. ISSN 21949050.

Bradstock, Ross A., 2009. Effects of large fires on biodiversity in south-eastern australia: disaster or template for diversity? Int. J. Wildland Fire 17 (6), 809–822.

Brede, Benjamin, Lau, Alvaro, Bartholomeus, Harm M., Kooistra, Lammert, 2017. Comparing riegl ricopter uav lidar derived canopy height and dbh with terrestrial lidar. Sensors 17 (10), 2371.

Brede, Benjamin, Calders, Kim, Lau, Alvaro, Raumonen, Pasi, Bartholomeus, Harm M., Herold, Martin, Kooistra, Lammert, 2019. Non-destructive tree volume estimation through quantitative structure modelling: Comparing uav laser scanning with terrestrial lidar. Remote Sens. Environ. 233, 111355.

Calders, Kim, Newnham, Glenn, Burt, Andrew, Murphy, Simon, Raumonen, Pasi, Herold, Martin, Culvenor, Darius, Avitabile, Valerio, Disney, Mathias, Armston, John, et al., 2015. Nondestructive estimates of above-ground biomass using terrestrial laser scanning. Methods Ecol. Evol. 6 (2), 198–208.

Cameron, Peter A., Mitra, Biswadev, Fitzgerald, Mark, Scheinkestel, Carlos D., Stripp, Andrew, Batey, Chris, Niggemeyer, Louise, Truesdale, Melinda, Holman, Paul, Mehra, Rishi, et al., 2009. Black saturday: the immediate impact of the february 2009 bushfires in victoria, australia. Med. J. Australia 191(1), 11-16.

Cao, Lin, Liu, Hao, Xiaoyao, Fu., Zhang, Zhengnan, Shen, Xin, Ruan, Honghua, 2019. Comparison of uav lidar and digital aerial photogrammetry point clouds for estimating forest structural attributes in subtropical planted forests. Forests 10 (2), 145.

Chen, Yang, Zhu, Xuan, Yebra, Marta, Harris, Sarah, Tapper, Nigel, 2016. Strata-based forest fuel classification for wild fire hazard assessment using terrestrial lidar. J. Appl. Remote Sens. 10 (4), 046025.

Clarke, Hamish G., Smith, Peter L., Pitman, Andrew J., 2011. Regional signatures of future fire weather over eastern australia from global climate models. Int. J. Wildland Fire 20 (4), 550–562.

Cooper, Sam, Roy, David, Schaaf, Crystal, Paynter, Ian, 2017. Examination of the potential of terrestrial laser scanning and structure-from-motion photogrammetry for rapid nondestructive field measurement of grass biomass. Remote Sens. 9 (6), 531.

Cruz, M.G., Matthews, S., Gould, J., Ellis, P., Henderson, M., Knight, I., Watters, J., 2010. Fire dynamics in mallee-heath: fuel, weather and fire behaviour prediction in south australian semi-arid shrublands. Bushfire Cooperative Research Centre, Report A, 10.

Cruz, M.G., Alexander, M.E., Plucinski, M.P., 2017. The effect of silvicultural treatments on fire behaviour potential in radiata pine plantations of south australia. For. Ecol. Manage. 397, 27–38.

Dandois, Jonathan P., Ellis, Erle C., 2013. High spatial resolution three-dimensional mapping of vegetation spectral dynamics using computer vision. Remote Sens. Environ. 136, 259–276.

Disney, M., Burt, A., Calders, Kim., Schaaf, C., Stovall, A., 2019. Innovations in ground and airborne technologies as reference and for training and validation: terrestrial laser scanning (tls). Surv. Geophy. 1–22.

Duff, Thomas J., Bell, Tina L., York, Alan, 2013. Predicting continuous variation in forest fuel load using biophysical models: a case study in south-eastern australia. Int. J. Wildland Fire 22 (3), 318–332.

Duff, Thomas J., Keane, Robert E., Penman, Trent D., Tolhurst, Kevin G., 2017. Revisiting wildland fire fuel quantification methods: the challenge of understanding a dynamic, biotic entity. Forests 8 (9), 351.

Duff, Thomas J., Cawson, Jane G., Penman, Trent D., 2019. Determining burnability: Predicting completion rates and coverage of prescribed burns for fuel management. For. Ecol. Manage. 433, 431–440.

Ellis, Stuart, Kanowski, Peter, Whelan, R.J., 2004. National inquiry on bushfire mitigation and management. Council of Australian Governments.

Fernandes, Paulo M., Botelho, Hermínio S., 2003. A review of prescribed burning effectiveness in fire hazard reduction. Int. J. Wildland Fire 12 (2), 117–128.

Fletcher, Andrew, Mather, Richard, 2020. Hypertemporal imaging capability of uas improves photogrammetric tree canopy models. Remote Sens. 12 (8), 1238.

Fritz, Andreas, Kattenborn, Teja, Koch, B., 2013. Uav-based photogrammetric point clouds—tree stem mapping in open stands in comparison to terrestrial laser scanner point clouds. Int. Arch. Photogramm. Remote Sens. Spat. Inf. Sci 40, 141–146.

García, Mariano, Mark Danson, F., Riano, David, Chuvieco, Emilio, Alberto Ramirez, F., Bandugula, Vishal, 2011. Terrestrial laser scanning to estimate plot-level forest canopy fuel properties. Int. J. Appl. Earth Observa. Geoinform. 13 (4), 636–645.

Gawel, Abel, Cieslewski, Titus, Dubé, Renaud, Bosse, Mike, Siegwart, Roland, Nieto, Juan, 2016. Structure-based vision-laser matching. In: IEEE International Conference on Intelligent Robots and Systems, 2016-Novem, pp. 182-188. doi: 10.1109/IROS.2016.7759053. ISSN 21530866.

Goldbergs, Grigorijs, Maier, Stefan W., Levick, Shaun R., Edwards, Andrew, 2018. Efficiency of individual tree detection approaches based on light-weight and low-cost uas imagery in australian savannas. Remote Sens. 10 (2), 161.

Goodbody, Tristan R.H., Coops, Nicholas C., White, Joanne C., 2019. Digital aerial photogrammetry for updating area-based forest inventories: A review of opportunities, challenges, and future directions. Curr. Forestry Rep. 5 (2), 55–75.

Gould, James Stanley, McCaw, W.L., Cheney, N.P., Ellis, P.F., Knight, I.K., Sullivan, A.L., 2008. Project Vesta: fire in dry eucalypt forest: fuel structure, fuel dynamics and fire behaviour. Csiro Publishing.

Graham, Alexander N.V., Coops, Nicholas C., Tompalski, Piotr, Plowright, Andrew, Wilcox, Mike, 2020. Effect of ground surface interpolation methods on the accuracy of forest attribute modelling using unmanned aerial systems-based digital aerial photogrammetry. Int. J. Remote Sens. 41 (9), 3287–3306.

Guo, Qinghua, Su, Yanjun, Hu, Tianyu, Zhao, Xiaoqian, Wu, Fangfang, Li, Yumei, Liu, Jin, Chen, Linhai, Xu, Guangcai, Lin, Guanghui, et al., 2017. An integrated uav-borne lidar system for 3d habitat mapping in three forest ecosystems across china. Int. J. Remote Sens. 38 (8–10), 2954–2972.

Hermosilla, Txomin, Ruiz, Luis A., Kazakova, Alexandra N., Coops, Nicholas C., Moskal, L. Monika, 2014. Estimation of forest structure and canopy fuel parameters from small-footprint full-waveform lidar data. Int. J. Wildland Fire 23 (2), 224–233.

Herrick, Jeffrey E., Schuman, Gerald E., Rango, Albert, 2006. Monitoring ecological processes for restoration projects. J. Nat. Conserv. 14 (3–4), 161–171. https://doi.org/10.1016/j.jnc.2006.05.001. ISSN 16171381.

Hill, Andreas, Breschan, Jochen, Mandallaz, Daniel, 2014. Accuracy assessment of timber volume maps using forest inventory data and lidar canopy height models. Forests 5 (9), 2253–2275.

Hillman, Samuel, Wallace, Luke, Reinke, Karin, Hally, Bryan, Jones, Simon, Saldias, Daisy S, 2019. A method for validating the structural completeness of understory vegetation models captured with 3d remote sensing. Remote Sens. 11 (18), 2118.

Hines, Francis, Hines, Francis, Tolhurst, Kevin G., Wilson, Andrew A.G., McCarthy, Gregory J., 2010. Overall fuel hazard assessment guide. Victorian Government, Department of Sustainability and Environment.

Höfle, Bernhard, Hollaus, Markus, Lehner, Hubert, Pfeifer, Norbert, Wagner, Wolfgang, et al., 2008. Area-based parameterization of forest structure using full-waveform airborne laser scanning data. In: Proceedings of SilviLaser, 2008: 8th.

Hollaus, Markus, Wagner, Wolfgang, Maier, Bernhard, Schadauer, Klemens, 2007. Airborne laser scanning of forest stem volume in a mountainous environment. Sensors 7 (8), 1559–1577.

Jain, Piyush, Wang, Xianli, Flannigan, Mike D., 1979. Trend analysis of fire season length and extreme fire weather in north america between 1979 and 2015. Int. J. Wildland Fire 26 (12), 1009–1020.

Jarron, Lukas R., Coops, Nicholas C., MacKenzie, William H., Tompalski, Piotr, Dykstra, Pamela, 2020. Detection of sub-canopy forest structure using airborne lidar. Remote Sens. Environ. 111770.

Jenkins, Meaghan E., Bedward, Michael, Price, Owen, Bradstock, Ross A., 2020. Modelling bushfire fuel hazard using biophysical parameters. Forests 11 (9), 925.

Matt Jolly, W., Cochrane, Mark A., Freeborn, Patrick H., Holden, Zachary A., Brown, Timothy J., Williamson, Grant J., Bowman, David M.J.S., 1979. Climate-induced variations in global wildfire danger from 1979 to 2013. Nat. Commun. 6 (7537), 2015.

Kilgore, Bruce M., Sando, Rodney W., 1975. Crown-fire potential in a sequoia forest after prescribed burning. For. Sci. 21 (1), 83–87.

Kramer, Heather A., Collins, Brandon M., Kelly, Maggi, Stephens, Scott L., 2014. Quantifying ladder fuels: a new approach using lidar. Forests 5 (6), 1432–1453.

Kramer, Heather A., Collins, Brandon M., Lake, Frank K., Jakubowski, Marek K., Stephens, Scott L., Kelly, Maggi, 2016. Estimating ladder fuels: a new approach combining field photography with lidar. Remote Sens. 8 (9), 766.

Liu, Kun, Shen, Xin, Cao, Lin, Wang, Guibin, Cao, Fuliang, 2018. Estimating forest structural attributes using uav-lidar data in ginkgo plantations. ISPRS J. Photogramm. Remote Sens. 146, 465–482.

Liu, Kun, Shen, Xin, Cao, Lin, Wang, Guibin, Cao, Fuliang, 2018. The evaluation of parametric and non-parametric models for total forest biomass estimation using uas-lidar. In: 2018 Fifth International Workshop on Earth Observation and Remote Sensing Applications (EORSA). IEEE, pp. 1–5.

Loudermilk, E. Louise, Kevin Hiers, J., O'Brien, Joseph J., Mitchell, Robert J., Singhania, Abhinav, Fernandez, Juan C., Cropper, Wendell P., Slatton, K. Clint, 2009. Ground-based lidar: a novel approach to quantify fine-scale fuelbed characteristics. Int. J. Wildland Fire 18 (6), 676–685.

Maguya, Almasi S., Tegel, Katri, Junttila, Virpi, Kauranne, Tuomo, Korhonen, Markus, Burns, Janice, Leppanen, Vesa, Sanz, Blanca, 2015. Moving voxel method for estimating canopy base height from airborne laser scanner data. Remote Sens. 7 (7), 8950–8972.

McColl-Gausden, S.C., Bennett, L.T., Duff, T.J., Cawson, J.G., Penman, T.D., 2020. Climatic and edaphic gradients predict variation in wildland fuel hazard in south-eastern australia. Ecography 43 (3), 443–455.

McElhinny, Chris, Gibbons, Phillip, Brack, Cris, Bauhus, Juergen, 2005. Forest and woodland stand structural complexity: its definition and measurement. For. Ecol. Manage. 218 (1–3), 1–24.

McLeod, Ron, 2003. Inquiry into the operational response to the january 2003 bushfires in the act. ACT Government, Canberra, ACT.

Menning, Kurt M., Stephens, Scott L, 2007. Fire climbing in the forest: a semiqualitative, semiquantitative approach to assessing ladder fuel hazards. Western Journal of Applied Forestry 22 (2), 88–93.

Newnham, Glenn J., Armston, John D., Calders, Kim, Disney, Mathias I., Lovell, Jenny L., Schaaf, Crystal B., Strahler, Alan H., Mark Danson, F., 2015. Terrestrial laser scanning for plot-scale forest measurement. Curr. Forestry Rep. 1 (4), 239–251. https://doi.org/10.1007/s40725-015-0025-5. ISSN 2198-6436.

Nyman, Petter, Sheridan, Gary J., Smith, Hugh G., Lane, Patrick N.J., 2011. Evidence of debris flow occurrence after wildfire in upland catchments of south-east australia. Geomorphology 125 (3), 383–401.

Olsoy, Peter J., Glenn, Nancy F., Clark, Patrick E., 2014. Estimating sagebrush biomass using terrestrial laser scanning. Rangeland Ecol. Manage. 67 (2), 224–228.

Ottmar, Roger D., Sandberg, David V., Riccardi, Cynthia L., Prichard, Susan J., 2007. An overview of the fuel characteristic classification system—quantifying, classifying, and creating fuelbeds for resource planning. Can. J. For. Res. 37 (12), 2383–2393.

Parsons, Russell A., Mell, William E., McCauley, Peter, 2011. Linking 3d spatial models of fuels and fire: effects of spatial heterogeneity on fire behavior. Ecol. Model. 222 (3), 679–691.

Pimont, François, Parsons, Russell, Rigolot, Eric, Coligny, François de, Dupuy, Jean-Luc, Dreyfus, Philippe, Linn, Rodman R., 2016. Modeling fuels and fire effects in 3d: model description and applications. Environ. Model. Softw. 80, 225–244.

Prichard, Susan J., Sandberg, David V., Ottmar, Roger D., Eberhardt, Ellen, Andreu, Anne, Eagle, Paige, Swedin, Kjell, 2013. Fuel characteristic classification system version 3.0: Technical documentation. Gen. Tech. Rep. PNW-GTR-887. Portland, OR: US Department of Agriculture, Forest Service, Pacific Northwest Research Station. 79, 2013, pp. 887.

Puliti, Stefano, Dash, Jonathan P., Watt, Michael S., Breidenbach, Johannes, Pearse, Grant D., 2019. A comparison of uav laser scanning, photogrammetry and airborne laser scanning for precision inventory of small-forest properties. Forestry: Int. J. Forest Res.

Rodríguez y Silva F., Molina, J.R., 2010. Manual técnico para la modelización de la combustibilidad asociada a los ecosistemas forestales mediterráneos. Departamento de Ingeniería Forestal. Universidad de Córdoba. Córdoba. España.

Eric Rowell, E., Loudermilk, Louise, Seielstad, Carl, O'Brien, Joseph J., 2016. Using simulated 3d surface fuelbeds and terrestrial laser scan data to develop inputs to fire behavior models. Can. J. Remote Sens. 42 (5), 443–459.

Rowell, Eric, Louise Loudermilk, E., Hawley, Christie, Pokswinski, Scott, Seielstad, Carl, Queen, Lloyd, O'brien, Joseph J., Hudak, Andrew T., Goodrick, Scott, Kevin Hiers, J., 2020. Coupling terrestrial laser scanning with 3d fuel biomass sampling for advancing wildland fuels characterization. For. Ecol. Manage. 462, 117945.

Salach, Adam, Bakuła, Krzysztof, Pilarska, Magdalena, Ostrowski, Wojciech, Górski, Konrad, Kurczyński, Zdzisław, 2018. Accuracy assessment of point clouds from lidar and dense image matching acquired using the uav platform for dtm creation. ISPRS Int. J. Geo-Inform. 7 (9), 342.

Sankey, Temuulen, Donager, Jonathon, McVay, Jason, Sankey, Joel B., 2017. Uav lidar and hyperspectral fusion for forest monitoring in the southwestern usa. Remote Sens. Environ. 195, 30–43.

Santosi, Zeljko, Sokac, Mario, Puskar, Tatjana, Budak, Igor, 2017. Comparative analysis of full frame and aps-c camera sensors on 3d digitization results. In: 2017 IEEE East-West Design & Test Symposium (EWDTS). IEEE, pp. 1–5.

Yilmaz, Cigdem Serifoglu, Yilmaz, Volkan, Güngör, Oguz, 2018. Investigating the performances of commercial and non-commercial software for ground filtering of UAV-based point clouds. Int. J. Remote Sens. 1–27. https://doi.org/10.1080/01431161.2017.1420942.

Skowronski, Nicholas, Clark, Kenneth, Nelson, Ross, Hom, John, Patterson, Matt, 2007. Remotely sensed measurements of forest structure and fuel loads in the pinelands of new jersey. Remote Sens. Environ. 108 (2), 123–129.

Snavely, Noah, Seitz, Steven M., Szeliski, Richard, 2007. Modeling the world from Internet photo collections. Int. J. Comput. Vision 80, 189–210. https://doi.org/10.1007/s11263-007-0107-3.

Spits, Christine, Wallace, Luke, Reinke, Karin, 2017. Investigating surface and near-surface bushfire fuel attributes: A comparison between visual assessments and image-based point clouds. Sensors 17 (4), 910.

Stephens, Scott L., McIver, James D., Boerner, Ralph E.J., Fettig, Christopher J., Fontaine, Joseph B., Hartsough, Bruce R., Kennedy, Patricia L., Schwilk, Dylan W., 2012. The effects of forest fuel-reduction treatments in the united states. Bioscience 62 (6), 549–560.

Sullivan, Andrew L., Lachie McCaw, W., Cruz, Miguel G., Matthews, Stuart, Ellis, Peter F, 2012. Fuel, fire weather and fire behaviour in australian ecosystems. Flammable Australia: fire regimes, biodiversity and ecosystems in a changing world, pp. 51–77.

Volkova, Liubov, Sullivan, Andrew L., Roxburgh, Stephen H., Weston, Christopher J., 2016. Visual assessments of fuel loads are poorly related to destructively sampled fuel loads in eucalypt forests. Int. J. Wildland Fire 25 (11), 1193–1201.

Vosselman, George, Gorte, Ben GH, Sithole, George, Rabbani, Tahir, 2004. Recognising structure in laser scanner point clouds. Int. Arch. Photogramm. Remote Sens. Spatial Inform. Sci. 46 (8), 33–38.

Wallace, Luke, Lucieer, Arko, Watson, Christopher, Turner, Darren, 2012. Development of a uav-lidar system with application to forest inventory. Remote Sens. 4 (6), 1519–1543.

Wallace, Luke, Watson, Christopher, Lucieer, Arko, 2014. Detecting pruning of individual stems using airborne laser scanning data captured from an unmanned aerial vehicle. Int. J. Appl. Earth Obs. Geoinf. 30, 76–85.

Wallace, Luke, Lucieer, Arko, Malenovskỳ, Zbyněk, Turner, Darren, Vopěnka, Petr, 2016. Assessment of forest structure using two uav techniques: A comparison of airborne laser scanning and structure from motion (sfm) point clouds. Forests 7 (3), 62.

Wallace, Luke, Bellman, Chris, Hally, Bryan, Hernandez, Jaime, Jones, Simon, Hillman, Samuel, 2019. Assessing the ability of image based point clouds captured from a uav to measure the terrain in the presence of canopy cover. Forests 10 (3), 284.

Wallace, Luke, Saldias, Daisy S., Reinke, Karin, Hillman, Samuel, Hally, Bryan, Jones, Simon, 2019. Using orthoimages generated from oblique terrestrial photography to estimate and monitor vegetation cover. Ecol. Indicators 101, 91–101.

Watson, Penny J., Penman, Sandra H., Bradstock, Ross A, 2012. A comparison of bushfire fuel hazard assessors and assessment methods in dry sclerophyll forest near Sydney, Australia. Int. J. Wildland Fire 21 (6), 755–763.

White, Joanne C., Wulder, Michael A., Vastaranta, Mikko, Coops, Nicholas C., Pitt, Doug, Woods, Murray, 2013. The utility of image-based point clouds for forest inventory: A comparison with airborne laser scanning. Forests 4 (3), 518–536.

Wieser, Martin, Mandlburger, Gottfried, Hollaus, Markus, Otepka, Johannes, Glira, Philipp, Pfeifer, Norbert, 2017. A case study of uas borne laser scanning for measurement of tree stem diameter. Remote Sens. 9 (11), 1154.

Wilkes, Phil, Jones, Simon D., Suarez, Lola, Haywood, Andrew, Mellor, Andrew, Woodgate, William, Soto-Berelov, Mariela, Skidmore, Andrew K., 2016. Using discrete-return airborne laser scanning to quantify number of canopy strata across diverse forest types. Methods Ecolo. Evol. 7 (6), 700–712.